Stack-and-draw applied to the engineering of multi-material fibers with non-cylindrical profiles

Clément Strutynski, Ricardo Alvarado Meza, Lionel Teulé-gay, Georges El-dib, Angeline Poulon-Quintin, Jean-paul Salvetat, Luc Vellutini, Marc Dussauze, Thierry Cardinal, Sylvain Danto

Stack-and-draw applied to the engineering of multi-material fibers with non-cylindrical profiles

Clément Strutynski[1], Ricardo Alvarado Meza[2], Lionel Teulé-Gay[1], Georges El-Dib[1], Angeline Poulon-Quintin[1], Jean-Paul Salvetat[3], Luc Vellutini[2], Marc Dussauze[2], Thierry Cardinal[1], Sylvain Danto[1*]

[1]CNRS, University of Bordeaux, Bordeaux INP, ICMCB, UMR 5026, Pessac, F-33600 France
[2]CNRS, University of Bordeaux, ISM, UMR-5255, Talence, F-33405 France
[3]PLACAMAT, CNRS, University of Bordeaux, UMS 3626, Pessac, F-33600 France

* **Corresponding Author :** *sylvain.danto@u-bordeaux.fr / orcid.org/0000-0002-3440-8288 / CNRS, University of Bordeaux, Bordeaux INP, ICMCB, UMR 5026, Pessac, F-33600 France.*

Abstract :

Here, it is demonstrated that the stack-and-draw approach can be expanded to unusual materials association and profile geometries to generate fiber assemblies with unprecedented functionalities. This approach relies on the stacking of flat oxide glass slides into a preform, which is then thermally elongated into tens-of-meters-long ribbon fibers with preserved cross-section ratio. Fabrication methodology is introduced. In order to illustrate the versatility of the method, a panel of fibers with diverse geometries and functions is exposed, including glass-only exposed-core fibers for chemical sensing and, upon the insertion of metal electrodes, H-shaped multi-cavity structures and compact, glass-metal fiber optical detectors applied to a gas analysis by means of fiber-tip plasma spectroscopy. It is believed this new approach will offer an attractive, straightforward solution for designing innovative, complex multimaterial fiber platforms with enhanced functionalities.

1. Introduction

Following the advent of ultralow-loss step-index silica optical fibers in the late seventies, the development of micro-structured optical fibers (MOF) enabled to alleviate the geometric limitation associated with all-solid, core-clad structures.[1-4] In micro-structured optical fibers, light wave guiding occurs thanks to a 2D periodic arrangement of air holes running along the main fiber axis.[5] Thanks to their unique propagating properties, micro-structured optical fibers found important applications ranging non-linear optics,[6] rare-earth doped fiber lasers or sensing.[7, 8] The success of micro-structured fibers relies vastly on the development and optimization of the stack-and-draw technique. This method consists in stacking together single “seed” glass rods into a macro-structured preform according to the desired cross-section pattern. Then the resulting assembly is scaled-down in size in a homothetic manner inside a drawing tower in order to preserve the original pattern in the final fiber optic. Besides light waveguide management in micro-structured fibers, the stack-and-draw technique enables the manufacturing of coherent fiber bundles for imaging and endoscopy.[9] This is nowadays a well-established technique for assembling materials such as silica glass but also tellurite glasses,[10] chalcogenide glasses,[11] or polymers[12, 13] into periodically arranged hollow fibers, usually originating from the use of circular amorphous “seed” rods.

In the current manuscript, we propose to revisit the well-established stack-and-draw technique. We demonstrate that the method can be expanded to unusual materials association and profile geometries to generate fiber assemblies with unprecedented functionalities. This approach relies on the stacking of flat soda-lime glass slides into a preform, which is then thermally elongated into tens-of-meters-long ribbon fibers with preserved cross-section. Emphasis is put on flat, ribbon-like fiber structures. Indeed, as fiber geometries are constantly evolving to overcome the numerous challenges related to integrated optics, they have recently emerged as a platform with strong potential for the development of smart monitoring devices with applications in photonics, dosimetry and others.[14, 15] They combine the advantages of fiber technology, namely flexibility, small footprint as well as interesting assets for planar optics. Functionalization of their high surface area is possible through the combination of various post-processing procedures such as Laser-based modifications,[16, 17] thermal poling, grafting with targeted molecules or even coating, which gives greater usefulness to the derived fibered system.

First, the main properties and key fabrication features of the newly developed method are introduced. Then, in order to highlight its versatility, a panel of fibers with diverse applications is exposed. The stack-and-draw technique is used to manufacture fibers with exposed waveguides subsequently decorated with a luminescent organic dye through click-chemistry processes to demonstrate its potential for bio-chemical sensing. Stepping forward, we move from the elaboration of glass-only made fibers to fibers embedding thin metallic wires within the soda-lime structures. H-shaped fiber structures comprising cavities, light-guiding core, and lateral metallic wires are then proposed. At last, an experimental development of compact, all-solid fiber optical detector applied to gas analysis by means of fiber-tip plasma spectroscopy is shown.

2. Revisiting the Stack-and-Draw Approach

The stack-and-draw technique consists in putting together glass rods and capillaries in order to form a preform which is subsequently elongated into tens-of-meters of optical fibers featuring regular patterned structures at the micrometer or even nanometer scale.[1, 2, 18] Usually the preform construction proceeds from cylindrical glass tubes or rods, stacked together in predetermined hexagonal lattice. This periodic arrangement of micrometric air holes running uniformly along the fiber length composes building blocks enabling to realize optical fiber devices with highly specific mode propagation properties.[9, 10, 19-22] In the current work, the stack-and-draw method is extended to the stacking of non-cylindric glass canes for the production of non-conventional all-glass or glass-metal fiber profiles. The fiber fabrication procedure encompasses three steps which are depicted in Figure 1. First, the glass pieces are processed into canes and plates with rectangular or square sections (Figure 1a). For this work, we employed standard silica-based vitreous materials, either prepared or commercially-available, with intermediate T_g. The different glass pieces are then stacked into non-conventional profiles as shown on Figure 1b. For the stack-and-draw method to be properly performed, cohesion must be brought to the preform. Traditionally, in MOF fiber fabrication route, the stack is inserted into a jacket tube, which brings stiffness to the capillary/cane bundle. This ensures cohesion of the stack and prevents the structure to partially or totally segregate during the heat-based drawing, as thermal expansion of each glass piece can cause severe distortion of the build. However, Dunn[10] demonstrated that a hexagonal stack of tellurite glass rods can be directly drawn without the need of an external tube when kept together by mechanical means (clamps and wirings). In the present study, cohesion of the stack is ensured by performing a consolidation treatment of the preform at $\approx T_g$ + 50 °C for 2 h prior to the elongation process (Figure 1b). During annealing, a moderate pressure (few kPa) is applied to the non-cylindrical stack causing the glass pieces to bond together. This process, also named fusion bonding,[23] is well known for glass–glass or silicon–glass wafers bonding. It is widely exploited for microfluidic chips fabrication, where two glass plates among which at least one is patterned, are assembled to form complex liquid paths at the micrometer scale. The bonding is efficient thanks to the presence of Si–OH entities at the surface of the different vitreous

slabs. When heated up, a reaction occurs leading to the formation of molecular H_2O and Si–O–Si bonds, with the later entities bridging the glass parts together.[24] The similar principle is exploited here for preform consolidation.

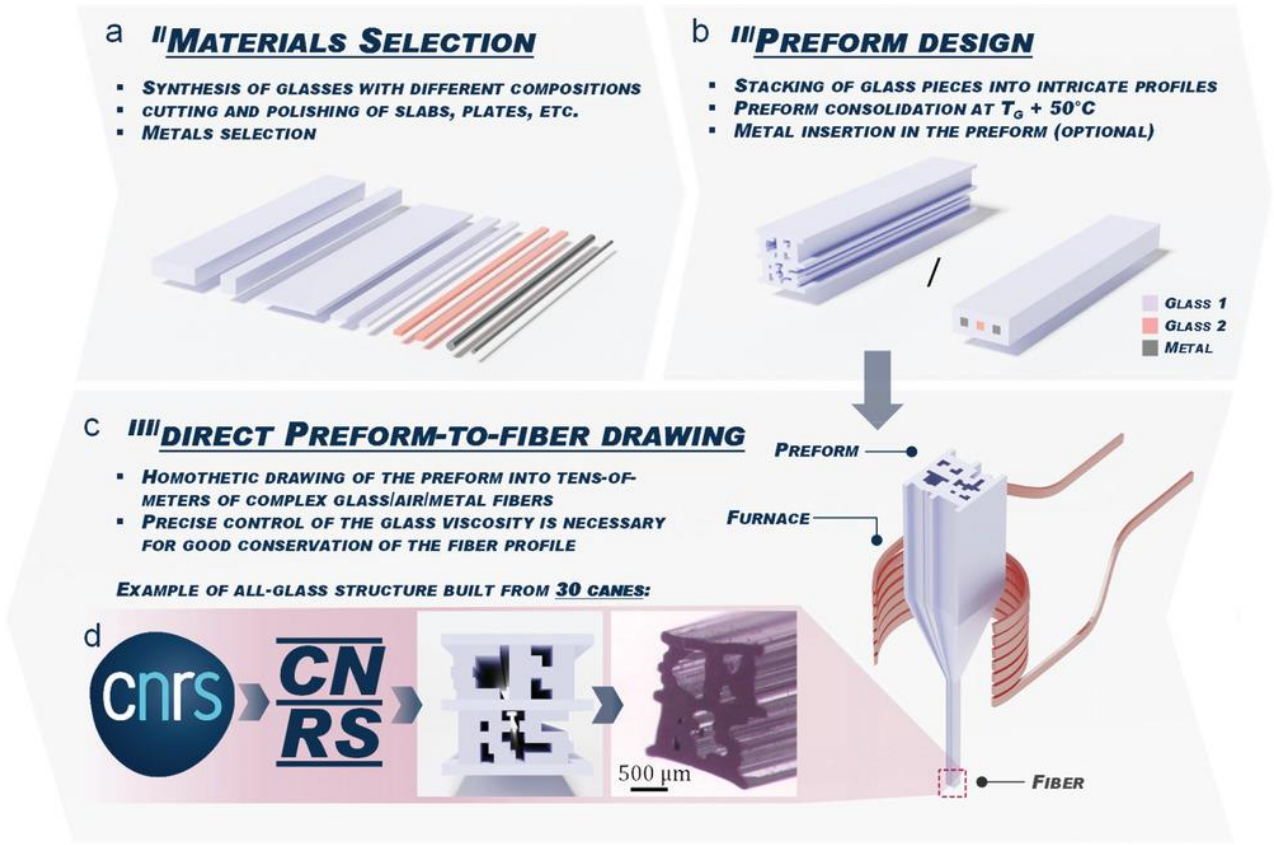

Figure 1 : *Description of the fabrication process of non-cylindrical composite fiber profiles using the stack-and-draw technique. It encompasses three steps: a) First, glasses with different compositions are processed (melting, cutting, and polishing) into canes, slabs, and plates. b) The glass pieces are stacked together to form a preform with an arbitrary complex profile. Then, the preform is annealed at T_g + 50 °C for consolidation purposes. c) Finally, it is thermally drawn into tens-of-meters long glass fibers. d) For demonstration purpose, a preform in the shape of the CNRS logo is made of 30 canes and is drawn into fiber.*

Finally, the built preform is thermally stretched down in homothetic fashion using a conventional draw tower. An example of fiber developed using this modified stack-and-draw technique is presented on Figure 1c. In order to highlight the full flexibility of the fiber fabrication route of the modified stack-and-fiber fabrication route, a 75-mm-long preform spatially arranged to spell the acronym "CNRS" (for "Centre National de la Recherche Scientifique") is built from 30 canes and plates with 1 × 2, 1 × 3, 1 × 4, 1 × 6 and 1 × 14 mm^2 rectangular sections. Optical microscope micrograph of the obtained fiber is presented in Figure 1d. The fiber cross-section is well preserved and does not exhibit any significant distortion, attesting for the potential of this newly-developed fabrication route for designing thermally-elongated structures with complex profiles.

In the following sections, we present a large panel of multi-material fibers fabricated by the stack-and-draw technique. These structures are built from standard soda-lime glass parts in the SiO_2–Na_2O–CaO–MgO–Al_2O_3 system (hereafter SiNaCa), used either as such (commercial) or upon composition tuning with Nb_2O_5 for refractive index tailoring (hereafter SiNaCa□Nb), and from commercially available metals (Zn, Al, Cu). The main properties of the considered materials are summarized in Table 1.

Table 1. Physical properties of the materials involved in the present work: Refractive index measured at 589 nm ($n@_{589nm}$), glass transition temperature (T_g), drawing temperature range (T_{Draw}), melting temperature (T_m), density (d), and electric resistivity (ρ).[25–27]

Name	$n@_{589\ nm}$ [±0.003]	T_g [±5 °C]	T_{Draw} [°C]	T_m [±5 °C]	D [±0.02 g cm^{-3}]	$\rho \times 10^{-9}$ [Ω m] at 20 °C
SiNaCa	1.522	577	750–800	—	2.48	—
SiNaCa-Nb	1.557	610	760–810	—	2.60	—
Zn	—	—	—	420	7.13	59.0
Al	—	—	—	660	2.70	26.5
Cu	—	—	—	1085	8.96	16.8

Based on the unusual material arrangements that offer the stack-and-draw approach, complex fiber profiles can be envisioned, providing a significant step toward more compact, Lab-on-fiber devices. In order to illustrate the versatility of the method, an example of fiber device combining dual electrical–optical functionalities is proposed (Figure 2). The assembly is composed of a rigid, flexible glass envelop embedding an optically-transparent glass core immerged in a channel and of two metallic electrodes running along its *z*-axis. The cavity can be subsequently filled with gases or liquid solutes for deported analyses.

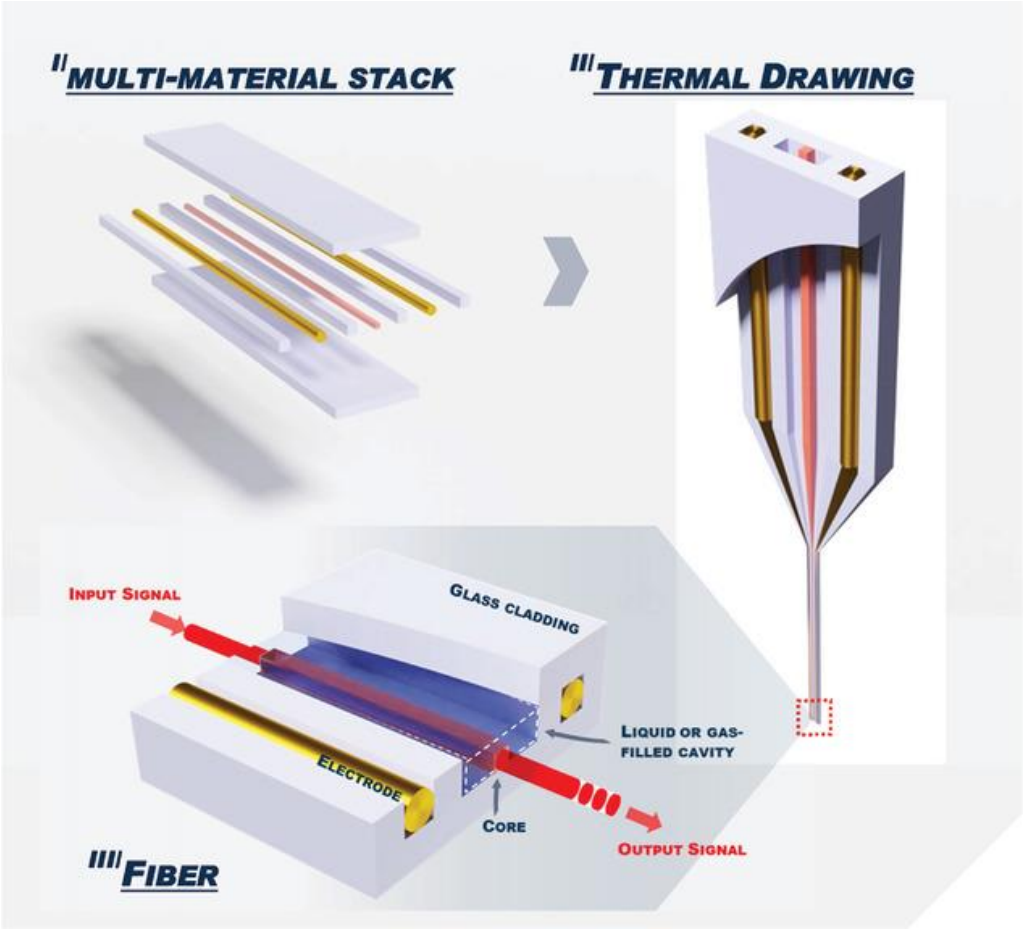

Figure 2 : *Proposed hollow, dual electrical–optical fiber device profile envisioned by the stack-and-draw technique. It is composed of a flexible glass envelop embedding an optically-transparent glass core immerged in a channel and of two metallic electrodes running along its z-axis.*

In the following sections, building blocks for the proposed proof-of-principle fiber profile are exposed.

3. Surface Functionalization of Ribbon Fibers with Exposed Waveguides

For sensing applications, the integration of waveguiding structures nearby the surface is key to maximize light/analyte interactions enhancing the device performances. Exposed-core or side-polished microstructured fibers are common solutions for such bare waveguide implementation,[28, 29] while, more recently, sensing solutions relying on near-surface laser-based inscription of refractive index modifications were also developed for similar purpose.[17] In this section, the stack-and-draw technique is used to propose an alternative path toward manufacturing of fibers with exposed waveguides. Following, the surface of the multi-glass elongated structure is successfully functionalized by an azide-terminated self-assembled monolayer (SAM) to covalently immobilized a luminescent organic dye through click-chemistry processes and its emission is detected through the fiber optical cores. The preform is composed of three Nb-loaded core glass canes which are disposed on a 3 × 15 × 75 mm cladding glass substrate and are separated by 1 × 3 × 75 mm^3 undoped glass canes (Figure 3a). The central and the two lateral cores have a 1 × 1 and 1 × 2 mm^2 section, respectively. The stack, annealed for consolidation as previously described, is subsequently drawn into meters of flat fiber, whose cross-section is displayed in Figure 3b. The overall shape of the initial preform is well preserved, with the three light-guiding high-index parts clearly visible on the micrograph. Dimensions of the central and lateral cores are respectively ≈16 × 16 μm^2 and ≈16 × 32 μm^2 while the outer dimensions of the fiber are 70 × 250 μm^2. The multi-glass structure then goes through a surface preparation process for the grafting of the fluorescent dye Cy5 (λ_{ex} 649 nm, λ_{em} 666 nm) (Figure 3c). For such functionalization, an organotrimethoxysilane (11-bromoundecyltrimethoxysilane) was grafted onto the surface of optical fiber to afford the corresponding bromine-terminated SAM. Then, this SAM-Br undergoes a modification of the terminal bromine substituted by an azide.[30, 31] The resulted azide-terminated SAM constitutes a universal reactive molecular platform to immobilize covalently (bio)molecular probe by an azide–alkyne click chemistry[32, 33] (See “Experimental” section for the full description of the fiber surface preparation mechanism).

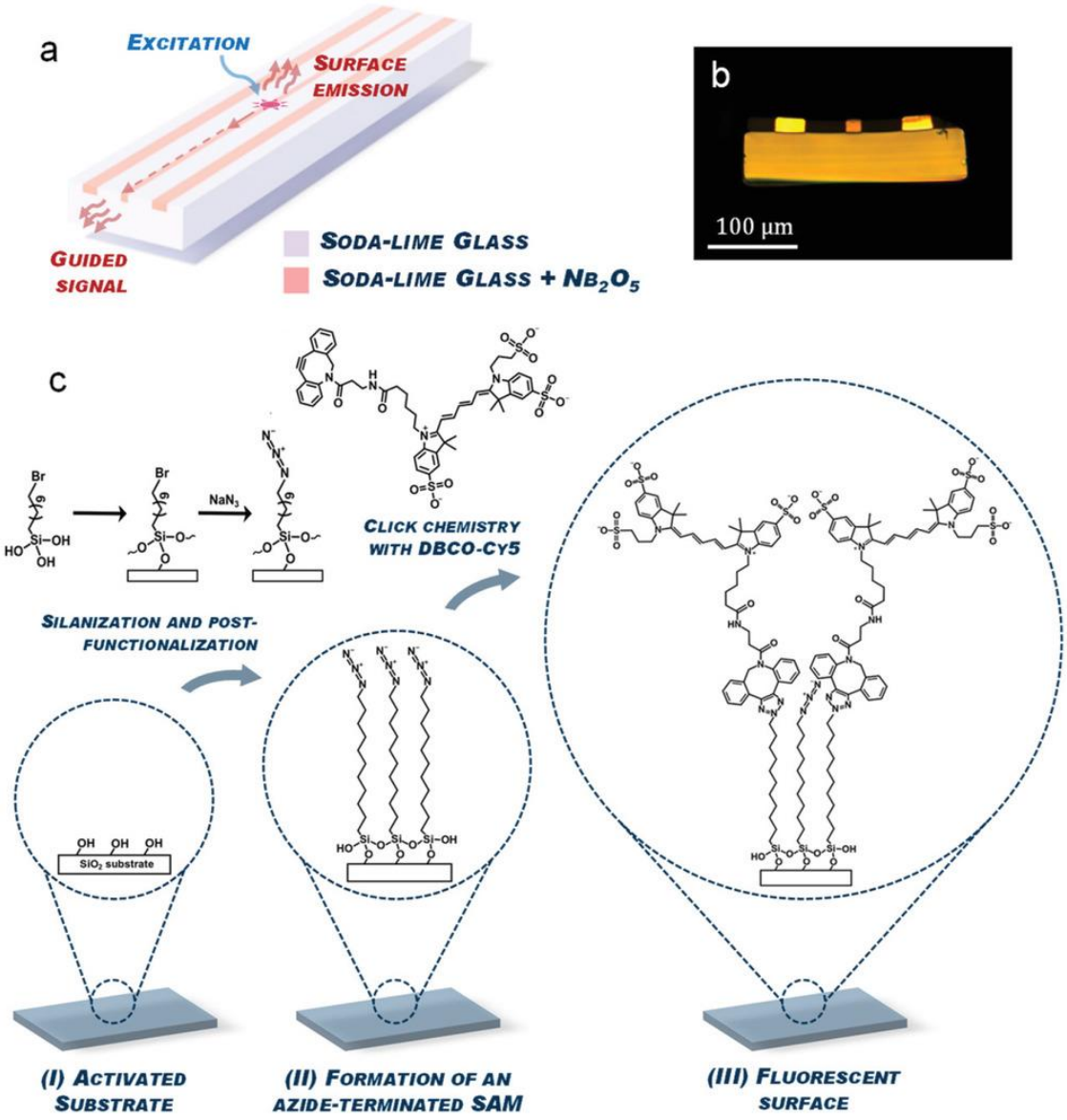

Figure 3 *: a) Description of the ribbon fiber possessing three surface waveguides. The fiber surface is functionalized with a luminescent dye and detection of both the surface luminescence and the guided signal is performed. b) Cross-sectional view of the ribbon fiber possessing three surface waveguides. The micrographs were captured using an optical microscope in transmission mode. c) Description of the surface functionalization approach.*

2D mapping of the emission of the Cy5 dye is then performed at the fiber surface using an HR evolution Raman spectrometer. More precisely, the microluminescence signal is collected on a ≈20 × 60 µm^2 area of the fiber surface with 0.5 µm steps in the *x* and *y* direction. Normalized integrational intensity (660–690 nm integration domain) with excitation at 633 nm is plotted in Figure 4a. A clear and relatively homogenous fluorescence signal, corresponding to the emission spectra of Cy5, is observed only on optical fibers with a SAM-N_3 exposed to DBCO-Cy5. Control assays with SAM-N_3 (before click chemistry) as well as fibers exposed to DBCO-Cy5 but with either a SAM-Br or without a SAM showed no fluorescence at all. These results suggest the successful grafting of organosilane derivatives as well as the specificity of the performed click reaction.

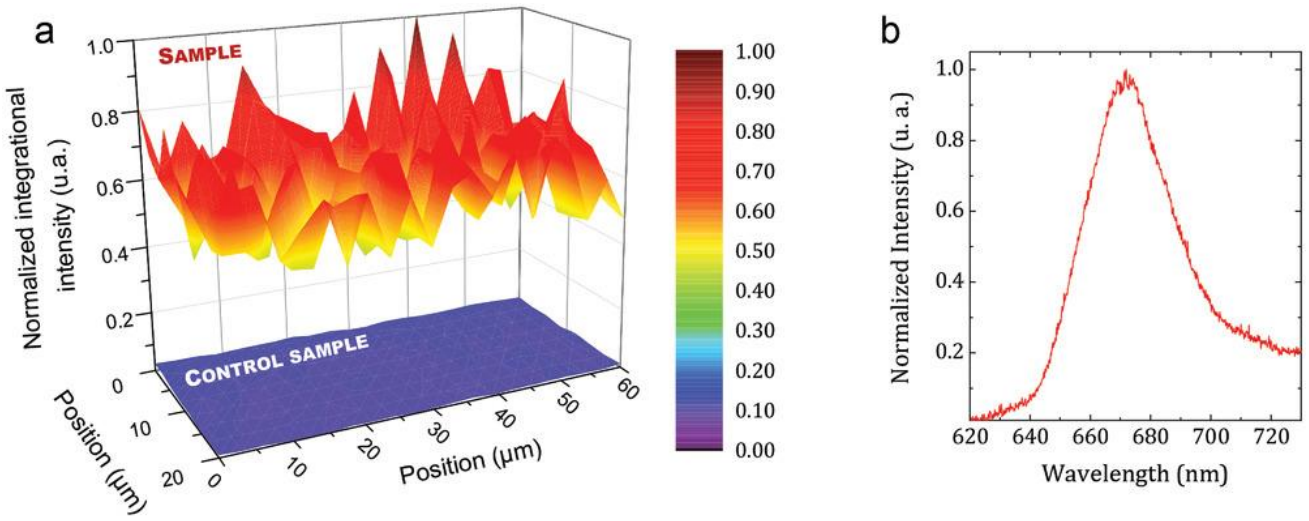

Figure 4 *: a) Normalized integrational intensity (660–690 nm integration domain) measured at the fiber surface on a ≈20 × 60 µm² area with excitation at 532 nm. For comparison, the same measurement was performed on a control sample (SAM-Br exposed to DBCO-Cy5) and the results are plotted here. b) Normalized signal recorded from one of the surface waveguides at one output end of the fiber sample when longitudinally excited at a wavelength of 589 nm.*

Then, in order to demonstrate the successful coupling of the emission signal of the Cy5 dye grafted on the surface into the exposed waveguides of the fiber, spectral analysis of the light carried toward the output of the elongated structure is performed. In this instance, the functionalized fiber is placed vertically on the HR Raman Spectrometer and is illuminated from the side with an external 589 nm light source (white light with bandpass filter) used as the optical excitation. A fraction of the light isotopically emitted from the dye is coupled into the waveguides and guided toward the fiber extremities. This signal is then retrieved by aligning the collection objective of the spectrometer with one of the surface waveguides at one end of the fiber. A typical normalized spectrum recorded in this manner is plotted on Figure 4b, displaying the characteristic red emission (centered at ≈675 nm) of the Cy5 dye. This result confirms the relevance of associating a dedicated fiber profile made by stack-and-draw with self-assembled monolayers for enabling future development of bio-chemical sensing devices.

4. Single Electrode Glass–Metal Fibers

While, in previous sections, we have considered glass-only fibers, here, stepping forward, we investigate the ability to embed thin metallic wires within the soda-lime structures. The considered wires, namely zinc, aluminum and copper, are inserted either in the preform prior to its fiber drawing or, post-drawing, into the fiber.

4.1 Zinc-Based Glass–Metal Fibers

As a first experiment, single electrode glass–metal fibers are drawn for feasibility demonstration purpose. The preform consists of a parallelepiped stack of soda–lime glass pieces with 11 × 8 × 75 mm^3 outer dimensions and possessing a central 2 × 2 × 55 mm^3 square hole which is fed with four 1 mm diameter zinc wires. Zinc is chosen here because of its moderate resistivity ($\rho_{Zinc} \approx 59 \times 10^{-9}$ Ω.m) as well as its thermal compatibility with the cladding glass ($T_{m\text{-}Zinc} < T_{Draw\text{-}glass}$). The build is thermally stretched down under argon at 750–800 °C into ≈400 × 550 µm² composite zinc/soda-lime fibers (Figure 5a inset). The DSC trace of the fabricated glass–metal fiber (red line) as well as the bare zinc electrode (black line) are plotted in Figure 5a. The DSC curve of Zn exhibits a sharp endothermic event at 424 °C corresponding to its melting point. If now considering the DSC trace of the glass–metal composite fiber, the position of zinc melting peak onset is at 423 °C, hence is in good agreement with the expected value of the bare metal.

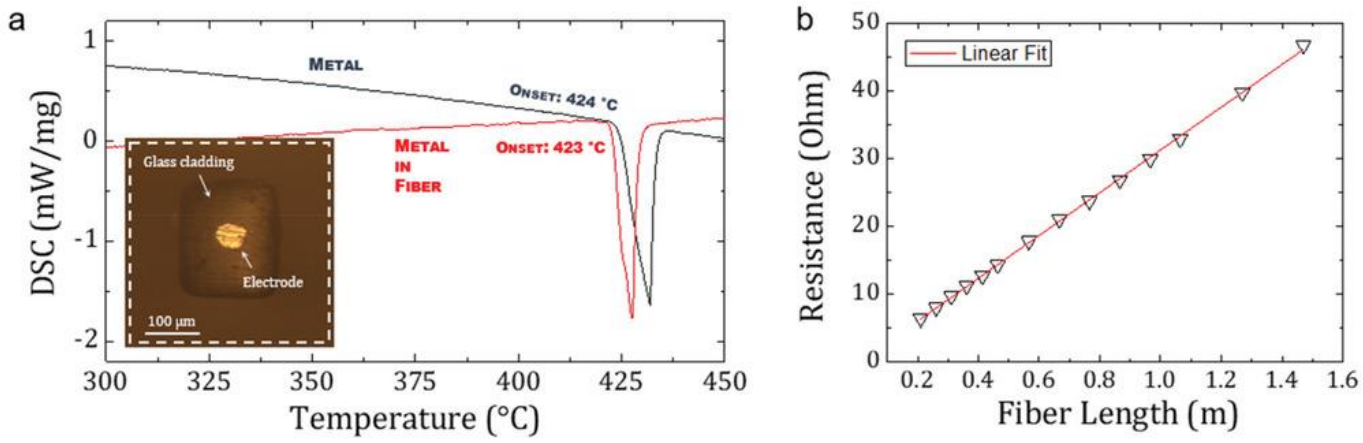

Figure 5 *: a) DSC curves of the bare Zn electrode (black line) and the glass–metal fiber (red line); Insert: Optical micrograph of the single electrode Zinc/soda–lime composite fiber. b) Plot of resistance as function of fiber length for an electrode of 50 µm diameter.*

The electric performance of the composite zinc/soda–lime fiber were then characterized by measuring resistance as function of the fiber length. Results are plotted in Figure 5b. The composite fiber shows a clear ohmic behavior, and linear regression of the discreet measurements gives information about zinc resistivity. Approximating the shape of the electrode to a cylinder of known diameter (50 µm), its resistivity is found to be 62×10^{-9} Ω m which is about 5% higher than the expected 59×10^{-9} Ω m value given in literature for zinc. This indicates that electric performances of the fiber are barely impaired.

4.2 Aluminum-Based Glass–Metal Fibers with Shaped Electrodes

Comparable experiments are carried out with Al/soda–lime composite fibers. With this materials combination however, precise control of the metallic electrode profile is possible. Aluminum is widely used in various industries because of its light weight and durability. Owing to its favorable weight to conductivity ratio, it is even preferred to copper in specific applications such as high-tension cables (better known as ACSR (aluminum conductor steel reinforced) cables) or to replace wiring in vehicles for weight reduction management. Besides, a large variety of aluminum alloys (Al–Cu, Al–Mg, Al–Si, Al–Sn, and more) are available and offer a broad range of physical properties (conductivity, melting temperature, tensile strength, and so on).[25]

In this sub-section, the preforms fabricated by stack-and-draw possess a central hole with a special shape which is again fed with 1 mm diameter Al wires. Exploded views of the different glass preforms are shown in Figure 6a1,b1,c1. The stacks are thermally stretched down into meters of composite glass/metal fibers with square-, strip-, or cross-shaped electrodes as shown in Figure 6a2–a4, b2–b4, and c2–c4 respectively. Remarkably, the shape on the initial electrode channel is very well preserved and sharp edge non-cylindrical metallic wires are successfully embedded in the fiber. This result strongly differs from the one obtained previously with Zn, where the square shape of the initial hole in the preform tends to transform into a cylindrical structure inside the fiber due to surface energy minimization (Figure 5a).

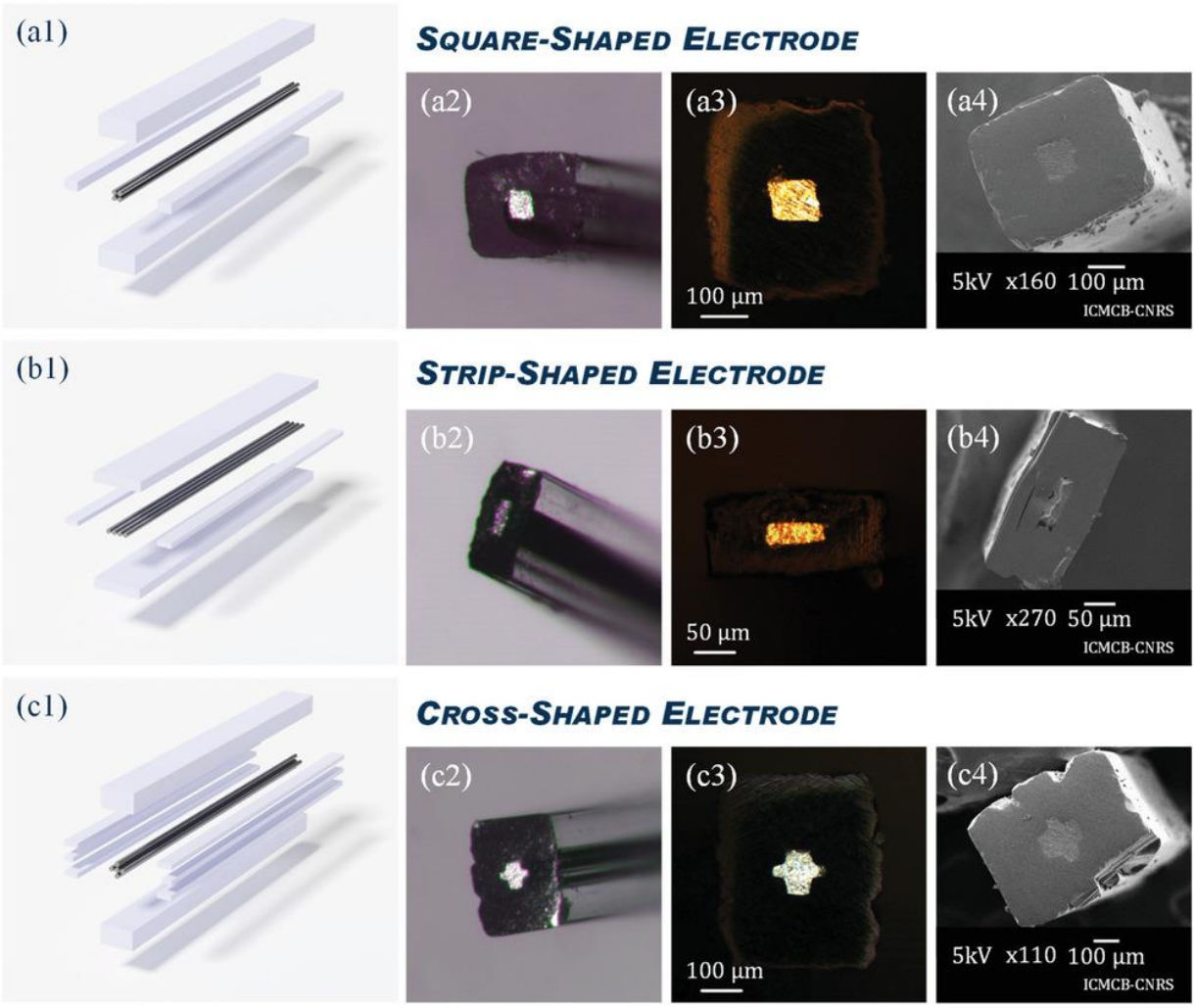

Figure 6 : *a1,b1,c1) Exploded views of the preforms studied in this section. Optical microscope observations and SEM micrograph of an Al/soda–lime composite fiber with a central electrode shaped into a a1–a4) square, b1–b4) strip, and c1–c4) cross.*

Such observation is due to the conditions in which the elongation process is performed. Draw tower furnaces generally possess sharp thermal profiles where the temperature is very high on a reduced area (few millimeters), with the neck-down region of the preform forming at the vicinity of this hot spot. By convention, the temperature at this position is considered as the drawing temperature T_{Draw}. When moving away from this area (above or below), temperature in the furnace $T_{Draw}(z)$ decreases but can remain moderately high on a significant distance covering the upper part of the preform. When considering the present molten core technique,[34-36] where the drawing temperature T_{Draw} exceeds the melting temperature $T_{m\ core}$ of a chosen core material, a hot melt forms inside the preform above the neck-down region. To some extent, the preform can be used as a crucible holding this melt where chemical reactions can occur, which allows for the synthesis of interesting compounds that are then directly embedded inside the fabricated fiber. This has been for instance exploited by Hou for the fabrication of crystalline silicon core fibers.[37] In the present case, the glass cladding acts as a support to restrict the flow of the molten metal. By gravity, it exerts a force on the surrounding cladding walls which depends on the weight of the melt above the glass softening region. Besides, depending on the drawing temperature and the core material melting temperature, the height and volume of the melt derived from the furnace temperature profile and the distance Δz on which $T_{Draw}(z) > T_{m\ core}$. Knowing this, the volume of molten material pushing down on the neck-down region should be smaller for Al as compared to Zn because of its higher melting temperature. Additionally, aluminum density is ≈2.6 times smaller than that of zinc (see Table 1). As a result, the force exerted by the hot liquid metal on the cladding glass through gravity is weaker in the case of aluminum. These observations explain

why Al is more practical than Zn to preserve the shape of the electrode when used as the central material. In similar glass viscosity regime and with comparable preform and fiber dimensions, action of liquid zinc on the glass walls is stronger and can cause important deformations of the final fiber structure. In this instance and in order to perfectly preserve the geometry, thermal drawing must be performed at higher viscosity, which can however mean sub-optimal conditions for the stretching of the glass. Alternatively, a drawing furnace with a sharper temperature profile is preferable.

DSC characterizations, performed on the raw Al metal as well as on the composite Al/soda–lime fiber, are plotted on Figure 7a. Similar to Zn (Figure 5a), the DSC traces of the bare metal (black line) and of the drawn metal (red line) exhibit a sharp endothermic event at 660 °C corresponding to the onset melting temperature of the aluminum. In fact, the melting peak is composed of two contributions whose onsets are found to be at 660 °C and 664 °C. This is related to impurities (most likely Fe or Nb) found in the source material used for the electrode. Fiber profile and chemical composition were checked thanks to time-of-flight secondary ion microscopy (ToF–SIMS) and energy-dispersive X-ray spectroscopy (EDX). For clarity, we show Al and Si measurements only. ToF–SIMS 2D mapping of the spatial repartition of Al^+ and Si^+ is performed at the vicinity of the Al/soda–lime interface (Figure 7b,c, respectively). SEM micrograph (magnification × 150) of the cross-sectional view of the fiber is depicted in Figure 7d along with the EDX spectroscopy analysis within the scanned area. Both methods, in good agreement between each other, reveal no chemical contamination or inter-diffusion occurring at the interface between the glass and the electrode material during the drawing process.

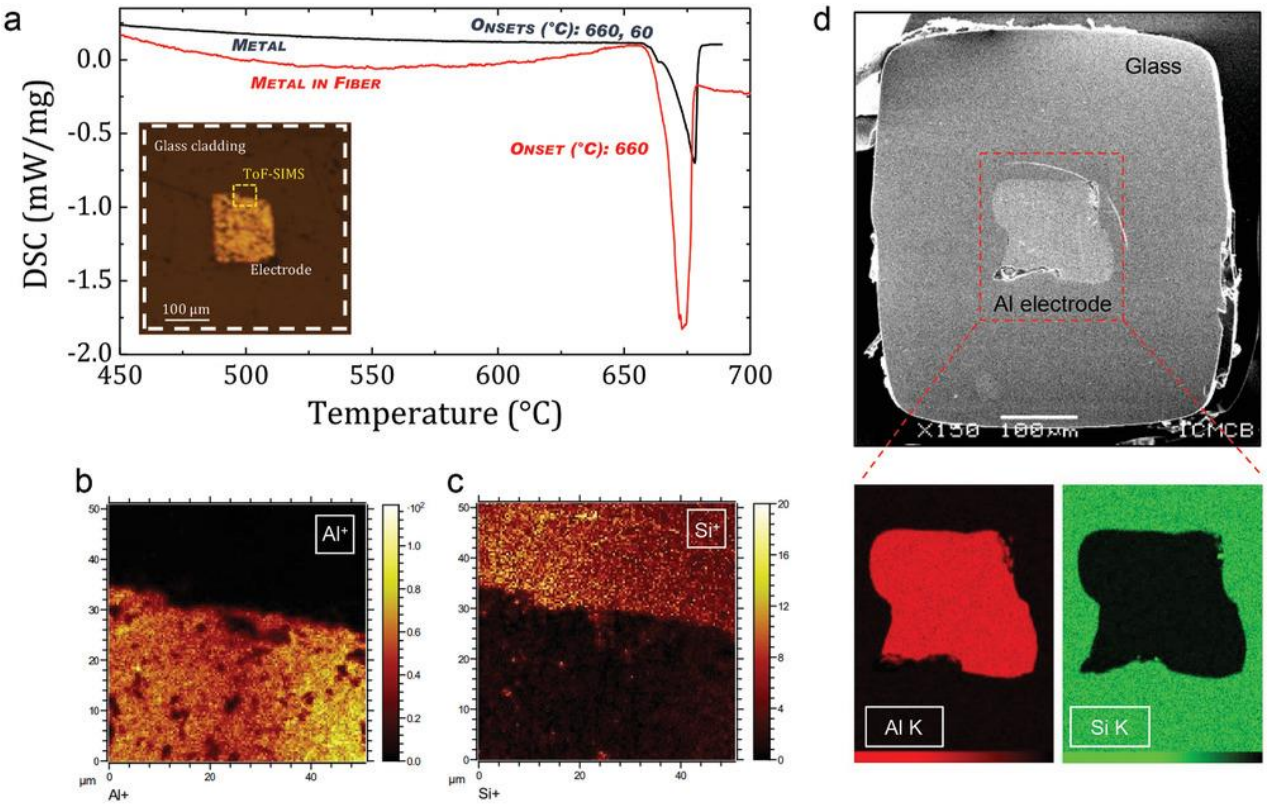

***Figure 7** : a) DSC curves of the bare Al electrode and the glass/metal fiber (insert: micrograph of the single electrode Al/soda–lime composite fiber). b,c) ToF–SIMS 2D mapping of the spatial repartition of, respectively, Al^+ and Si^+ at the vicinity of the glass–metal interface. d) Energy-dispersive X-ray spectroscopy analysis of Al electrode.*

At this stage of the study, further electrical characterizations of the fiber could not be performed as conventional electrical contacts of the fiber could not be implemented. Because of the small contact area and of the Al_2O_3 layer

naturally forming at the exposed surface of the electrode, classical methods (electrically-conductive paints or tin soldering) appeared unpractical. Continuity of the fiber was however demonstrated by connecting both ends of a 10 cm long fiber with an InGa alloy which is liquid at room temperature. The alloy reacts with aluminum and an electric contact can be made in this manner. A resistance of 17 kΩ was measured on the 10 cm long fiber, proving the continuity of the embedded Al wire. No further information about the resistivity of the electrode could be extracted in this instance due to the high and unstable contact resistance. Other electric connection methods will be considered, such as the use of probe station or laser-based soldering solutions.

Nevertheless, despite the work remaining for integrating such Al/soda–lime fibered builds in operational electro-optic devices, the ability to shape metallic electrodes embedded inside fibers still remains highly attractive. This would allow for the precise spatial shaping of electric fields for the triggering of specific electro-optic phenomena. It could benefit for instance to the development of endoscopic probes, especially for electrochemotherapy applications. Tremendous efforts are carried out in this research area concerning the geometry of the probes which must provide precisely tailored electric field distributions at their tips for improved cancer treatment.[38, 39]

5. Light-Guiding, Dual-Electrode Fibers with Internal Rectangular Cavity

Preforms manufactured by the stack-and-draw technique commonly possess channels which are kept empty inside the stack-and-form conduits in the subsequently drawn fiber. Those air gaps play an important role for light-guiding purposes but can also be filled with various materials. Nonlinear processes based on light-matter interactions can for instance be enhanced by filling the holes of precisely tailored micrometric structures with gases.[40, 41] Electrolyte-filled hollow fibers are also used in microprobe development for in vivo recordings.[42] More interestingly, solid metallic wires can be inserted in the holes or even liquid metal can be forced into them to add electrical functionalities to the fiber.[43, 44] Figure 8a describes an all-glass hollow fiber manufactured by the stack-and-draw technique to which copper wires are added post-drawing to the fiber. Micrograph of the section of the initial fiber is shown on Figure 8b. A light-guiding core is laying inside an empty cavity and two slots are positioned on each side of the structure in order to hold metallic wires. Figure 8c shows a longitudinal view of the fiber with two implanted copper wires which are epoxy-glued to the glass structure to hold them in place. Incorporation of metals after the elongation process is an alternative to the direct preform-to-fiber drawing method described in the previous section. It allows for instance for the use of metal with interesting properties (conductivity, chemical reactivity, and others) but which are not thermally compatible with the cladding glass, that is, with $T_{m\text{-}metal} > T_{Draw\text{-}glass}$. It also simplifies connection of the metallic electrodes as well as of the fiber processing in general (cleaving). Despite the wide combinations of materials enabled by this two-step approach, it reveals to be impractical to some extent, as scalability and repeatability of the process are limited. Finally, a similar fiber geometry is fabricated by the direct preform-to-fiber drawing method, as described in Figure 8d. This time zinc wires are fed in the lateral holes of the preform prior to the elongation process and are directly co-drawn with the soda–lime glass in a single-step. Micrographs of the fabricated glass–metal fiber in reflection and transmission mode are shown in Figure 8e,f respectively.

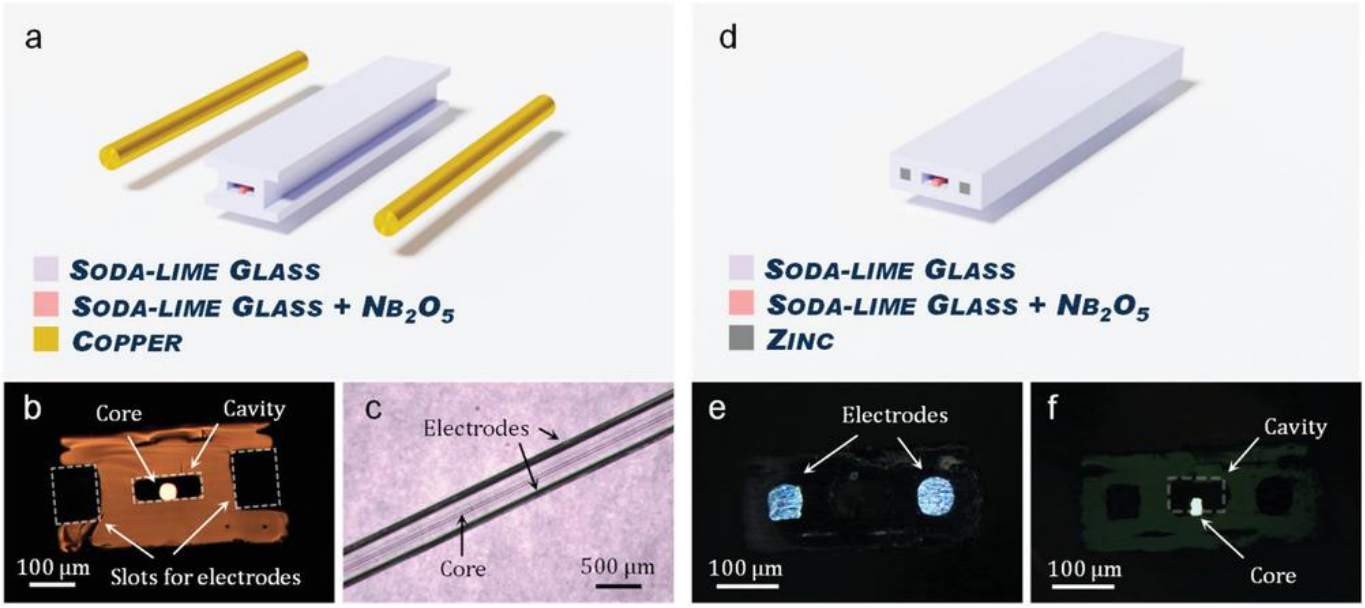

Figure 8 *: a) Description of a H-shaped hollow fiber with a light-guiding core laying in a rectangular cavity. The fiber possesses two lateral slots running along its body for metallic wire insertion post fiber-drawing. b) Cross-sectional view of the H-shaped fiber in transmission mode. c) Longitudinal view of the H-shaped fiber with two copper wires inserted in the slots provided for that purpose. d) Description of a dual-electrode hollow glass–metal fiber with its light-guiding core laying in a rectangular cavity. Micrographs of the cross-section of the directly drawn fiber recorded using an optical microscope in e) transmission mode and f) reflection mode.*

Implementation of intricate micrometric geometries within fibers is proven possible with the revisited stack-and-draw technique. The ability to blend materials with disparate optical and electrical properties within glass fibers opens new opportunities for increasing the complexity of fiber architectures. Further experimentations involving interesting light-matter interactions occurring under electric fields within such composite builds are currently under progress.

6. Plasma Generation at the Tip of a Dual-Electrode Core-Cladding Fiber

Taking advantage of the widely available possibilities enabled by the stack-and-draw method for the fabrication of glass–metal fibers, a more sophisticated structure featuring both optical and electrical assets is considered in this section. In a previous work, the authors have demonstrated the successful implementation of an optical emission detector based on the generation of plasma at the tip of a fiber assembly.[45] The proof of principle device relies on a polymer/metal fiber for discharge generation associated with a commercial multimode fiber (MMF) for signal collection. More precisely, to form the sensor, the MFF is inserted inside the central hole of the hollow tin/PES (PolyEther Sulfone) elongated structure which is fabricated by the direct preform-to-fiber drawing process. In this section, a similar detection system is fabricated in a single-step operation using the stack-and-draw technique.

Description of the all-solid glass–metal fiber produced for this purpose is given in Figure 9. It consists in a ≈100 × 100 µm^2 square glass core surrounded by two ≈100 µm diameter metallic electrodes separated by a 300 µm gap. Dimensions of the rectangular outer cladding are ≈300 × 700 µm^2. Commercial float glass is used as the cladding material while high refractive index Nb_2O_5-doped soda–lime glass is used for the core. Sufficient refractive index difference between the core and the cladding glasses ensures the guiding of light within the central core, as reported in Table 1. Additionally, the glass cladding possesses a high dielectric strength (around 15.5 kV mm^{-1} [46]) as well as moderate thermal resistance (T_g > 500 °C), which means it can sustain the physical effects (elevated voltage, heat, etc.) related to the high potential discharge generation. The electrodes embedded

in the structure are made of zinc. Cross-sectional views of the multi-material fiber taken with an optical microscope in transmission and reflection mode respectively are shown in Figure 9c,d.

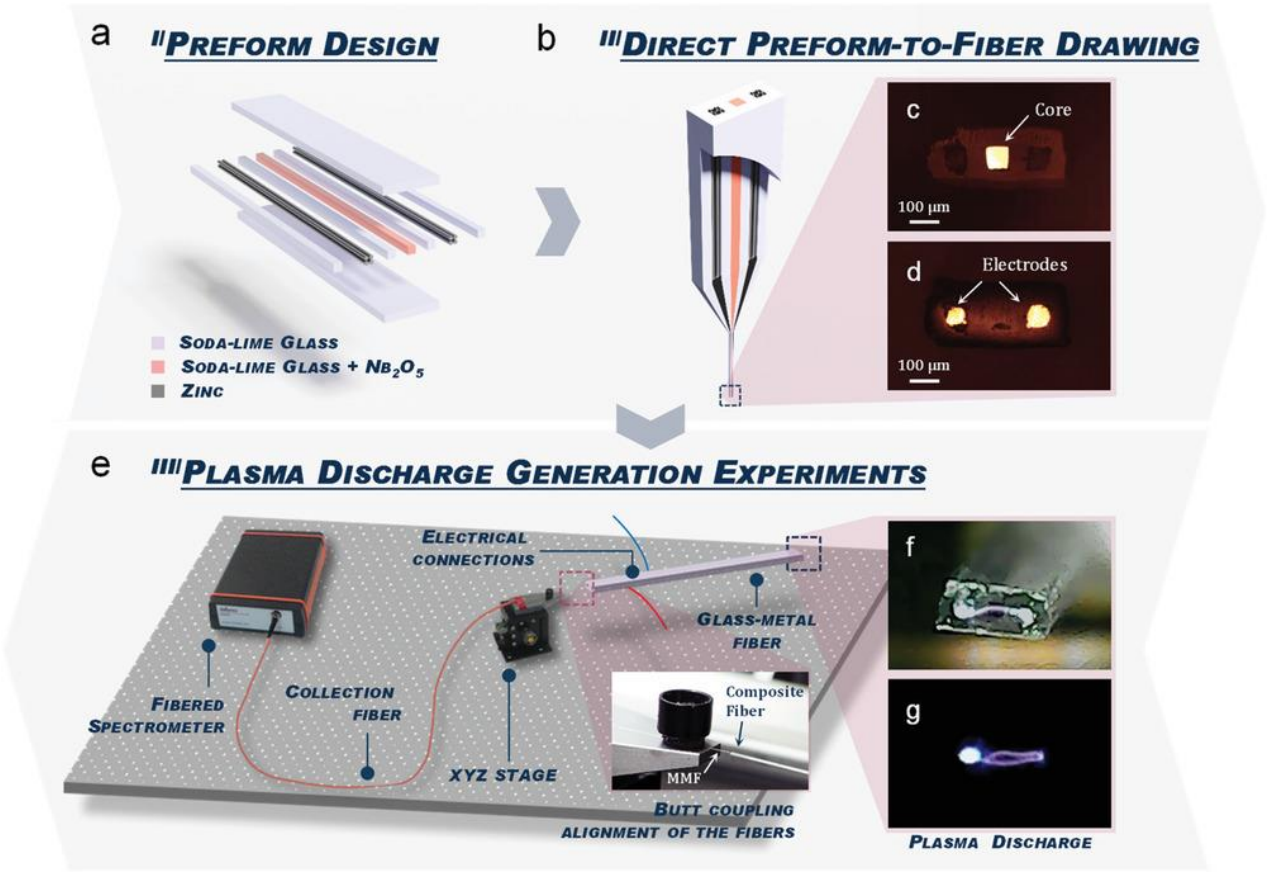

Figure 9 *: a) Exploded view of the glass–metal preform fabricated by the stack-and-draw technique. b) Direct preform-to-fiber drawing of the preform into meters of composite fiber. Micrographs of the core-cladding dual-electrodes fiber recorded using an optical microscope in c) transmission mode and d) reflection mode. e) Scheme of the experimental setup used for plasma discharge generation. Pictures of the plasma generated at the tip of the fiber taken in different lighting conditions: f) white light illumination and g) in the dark.*

For further experimentations, external adjacent connection of the embedded electrodes is performed by polishing the side of the fiber and attaching 100 µm diameter copper wires to the exposed Zn electrodes with silver paint. The electric contacts are then connected to a DC generator (Branderburg AlphaIII) for plasma discharge generation. In the present experimental conditions, namely at atmospheric pressure with a 300 µm gap between the two electrodes, a potential of 1.5 kV was enough to obtain a discharge at the tip of the fiber. Pictures of the plasma taken with white light illumination and in the dark are presented on Figure 9f,g respectively. The discharge running between the electrodes shines in front of the waveguiding optical core of the fiber in which light is coupled. Signal is collected in this manner and is further guided toward the other extremity of the composite fiber which is butt-coupled to a commercial silica multimode optical fiber.

Description of the experimental setup is given on Figure 9e. The MMF is directly plugged to a UV–vis-NIR fibered spectrometer (Avantes AvaSpec-ULS4096CL-EVO) which is used to record the collected signal between 200 and 1100 nm. A typical spectrum registered from the setup described here is displayed in Figure 10. Signatures from the main constituents of air, namely nitrogen, oxygen and argon, can be identified.[47] A hydrogen related emission is also visible on the spectra around 650 nm due to the presence of moisture in the probed atmosphere. This device can be exploited to differentiate various atmospheres as proven in a previous study carried out in a similar configuration.[45] More importantly, those results prove that useful intricate fiber profiles can be developed from the revisited stack-and-draw technique.

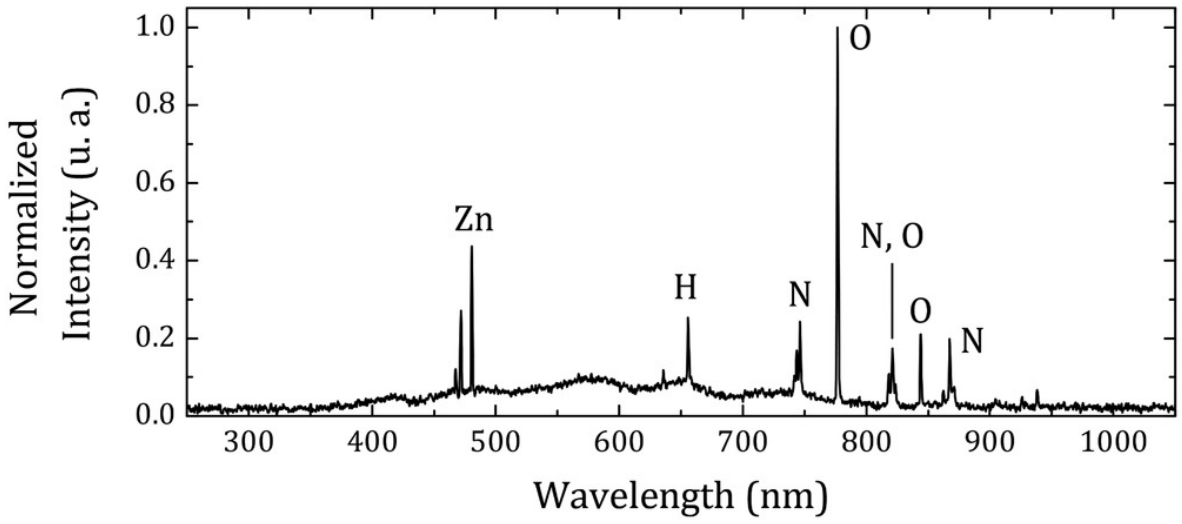

Figure 10 *: A typical spectrum collected from the proof-of-principle optical emission detector when placed in ambient air.*

7. Conclusion

In this article, a modified stack-and-draw approach is proposed to elaborate multimaterial, multifunctional fiber devices with complex profiles geometries and integration. The method consists in the direct, homothetic thermal drawing of a stack of rectangular soda–lime glass parts organized into a functional preform. Waveguide detection of fluorescence at the surface of the fiber was demonstrated, suggesting that this system can be further exploited in the development of bio-chemical sensing devices. Upon the insertion of metal electrodes, a compact fiber optical gas analyzer based on fiber-tip plasma spectroscopy is shown. This fiber fabrication strategy represents a new, versatile method offering numerous degrees-of-freedom in the materials selection and their respective arrangement. Beside common silica-based vitreous materials, the method can be extended to other specialty glass matrices with interesting physico-chemical assets such as extended transmission in the IR, enhanced nonlinear optical properties, photo-sensitivity or others. Glasses can also be combined with polymers or metals, while cavities, subsequently filled with gases or fluids, can be inserted to the structure to expand even further the range of possible applications.

In the search for developing a multi-functional, compact Lab-on-fiber device, we believe the stack-and-draw approach exposed here represents a significant step ahead. Indeed, it offers an attractive, straightforward solution for designing innovative, complex multimaterial fiber platforms with enhanced functionalities, dedicated for instance to highly-efficient sensors of biomolecules of interest, to microfluidic devices owing multiple channels, but also to fiber-based devices where a dual electrical-optical function is sought for.

8. Experimental Section

Glass Synthesis

Glasses in the system SiO_2–Na_2O–CaO–MgO–Al_2O_3 tailored with Nb_2O_5 were prepared to obtain vitreous samples with targeted properties (increased refractive index, etc.). To do so, commercial soda–lime float glass pieces were remelted with niobium oxide in the powder form. The mix was ground and heated at 1550 °C in an electric furnace for 24 h. During the synthesis, several quenching and grinding operations were carried out in order to ensure good homogeneity of the glass. The melt was then poured inside a 20 × 25 × 65 mm^3 rectangular brass mold preheated at 500 °C. The glass ingots were subsequently annealed at 540 °C for 5 h after which the

temperature was slowly ramped down (2 °C min^{-1}) to room temperature. The parallelepiped shape of the samples offered practical advantages for the post-processing steps of cutting and polishing. A typical glass piece approximately weighs 80 g and can be cut into few tens of smaller canes (with rectangular or square sections) or plates which are then used for the fabrication of glass preforms. Additionally, commercial float glass slabs are processed in the same manner to complete the set of available glass pieces.

Fiber Drawing

After the glass synthesis and processing, the fabricated canes were stacked together into non-cylindrical macroscopic air/glass preforms. The glass bundle was then drawn under an Ar flow (2 L min^{-1}) using a dedicated 3 m high draw tower at 750-800°C. First the preform was heated up to its softening temperature at 10 °C min^{-1} to initiate the elongation process. After that, the stack was slowly fed into the furnace while the drawing parameters were continuously monitored to produce a fiber with targeted dimensions. Fine control of the glass viscosity was crucial for the stretching of the complex non-cylindrical structures which were described in this work.

Grafting of the Fluorescent Dye Cy5 on Fiber Surface

The azide-terminated SAM was prepared according to the literature.[31] The optical fibers were rinsed with Milli-Q water (18 MΩ.cm), sonicated for 15 min in $CHCl_3$, and activated by a 30 min exposure to UV/O_3. The optical fibers were immersed in a silanization flask under an inert atmosphere (N_2) and exposed for 16 h to a solution containing 11-bromoundecyltrimethoxysilane (5×10^{-5} mol) synthesized according to literature and trichloroacetic acid (TCA, 5×10^{-6} mol) in 200 mL of anhydrous toluene at 20 °C.[30] The fibers were then rinsed by multiple cycles of 5 min sonication in toluene, water, and chloroform (twice per solvent) and dried under nitrogen flow. The bromide moieties of the SAM were then replaced via nucleophilic substitution with azide by immersing the fibers in a saturated solution of NaN_3 on anhydrous DMF for 48 h at room temperature under an inert atmosphere. Fibers were then rinsed by multiple cycles of 5 min sonication in DMF, water, and $CHCl_3$ (twice per solvent). Finally, conjugation with a fluorescent dye was done via Strain-Promoted Alkyne–Azide Cycloaddition (SPAAC) which consisted in the exposure of the functionalized fibers to a 6×10^{-6} m solution of DBCO-Cy5 in water at room temperature overnight. Finally, the fibers were sonicated in cycles of 5 min on water and $CHCl_3$.

Acknowledgements : Funding for this work was provided from the French Government, managed by the French National Research Agency (ANR Grant #62243) and the CPER Campus B, by the Program IdEx at the University of Bordeaux, the Cluster of excellence LAPHIA, and by the Région Nouvelle-Aquitaine.

Conflict of Interest : The authors declare no conflict of interest.

Data availability statement : Research data are not shared.

Reference

1- P. Russell, *Science* 2003, 299, 358.

2- T. M. Monro, H. Ebendorff-Heidepriem, *Annu. Rev. Mater. Res.* 2006, 36, 467.

3- J. C. Knight, T. A. Birks, P. S. J. Russell, D. M. Atkin, *Opt. Lett.* 1996, 21, 1547.

4- T. A. Birks, J. C. Knight, P. S. J. Russell, *Opt. Lett.* 1997, 22, 961.

5- T. M. Monro, in Guided Wave Optical Components and Devices (Ed: B. P. Pal), Elsevier, Amsterdam, the Netherlands 2006, pp. 41– 70.

6- T. Nakanishi, I. Hirano, T. Okuno, M. Onishi, in Optical Fiber Communication Conference and Exposition and The National Fiber Optic Engineers Conference, Optical Society of America, Washington 2006, p. OTuH7.

7- A. Candiani, A. Cucinotta, in Optofluidics, Sensors and Actuators in Microstructured Optical Fibers (Eds: S. Pissadakis, S. Selleri), Elsevier, Amsterdam, the Netherlands 2015, pp. 229– 246.

8- J. H. V. Price, K. Furusawa, T. M. Monro, L. Lefort, D. J. Richardson, *J. Opt. Soc. Am. B* 2002, 19, 1286.

9- J. M. Stone, H. A. C. Wood, K. Harrington, T. A. Birks, *Opt. Lett.* 2017, 42, 1484.

10- C. Dunn, F. Kong, G. Gu, T. W. Hawkins, M. J. Jones, A. Runnion, M. T. Kalichevsky-Dong, R. Salem, D. Liu, D. Gardner, P. Fendel, R. Synowicki, E. Cheung, J.-T. Gomes, L. Lavoute, D. Gaponov, S. Février, L. Dong, *Fibers* 2017, 5, 37.

11- J. Troles, L. Brilland, in Chalcogenide Glasses (Eds: J.-L. Adam, X. Zhang), Elsevier, Amsterdam, the Netherlands 2014, pp. 411– 437.

12- M. van Eijkelenborg, M. Large, A. Argyros, J. Zagari, S. Manos, N. Issa, I. Bassett, S. Fleming, R. McPhedran, C. M. de Sterke, N. A. Nicorovici, *Opt. Express* 2001, 9, 319.

13- M. A. van Eijkelenborg, A. Argyros, G. Barton, I. M. Bassett, M. Fellew, G. Henry, N. A. Issa, M. C. J. Large, S. Manos, W. Padden, L. Poladian, J. Zagari, *Opt. Fiber Technol.* 2003, 9, 199.

14- C. Holmes, S. Ambran, P. A. Cooper, A. S. Webb, J. C. Gates, C. B. E. Gawith, J. K. Sahu, P. G. R. Smith, *Meas. Sci. Technol.* 2020, 31, 085203.

15- A. Alawiah, S. Bauk, H. A. Abdul-Rashid, W. Gieszczyk, S. Hashim, G. A. Mahdiraji, N. Tamchek, D. A. Bradley, *Radiat. Phys. Chem.* 2015, 106, 73.

16- S. Danto, F. Désévédavy, Y. Petit, J.-C. Desmoulin, A. Abou Khalil, C. Strutynski, M. Dussauze, F. Smektala, T. Cardinal, L. Canioni, *Adv. Opt. Mater.* 2016, 4, 162.

17- A. A. Khalil, P. Lalanne, J.-P. Bérubé, Y. Petit, R. Vallée, L. Canioni, *Opt. Express* 2019, 27, 31130.

18- J. J. Kaufman, G. Tao, S. Shabahang, D. S. Deng, Y. Fink, A. F. Abouraddy, *Nano Lett.* 2011, 11, 4768.

19- P. S. J. Russell, *J. Lightwave Technol.* 2006, 24, 4729.

20- F. Stutzki, F. Jansen, H.-J. Otto, C. Jauregui, J. Limpert, A. Tünnermann, *Optica* 2014, 1, 233.

21- F. Luan, A. K. George, T. D. Hedley, G. J. Pearce, D. M. Bird, J. C. Knight, P. S. J. Russell, *Opt. Lett.* 2004, 29, 2369.

22- A. L. Bullington, P. H. Pax, A. K. Sridharan, J. E. Heebner, M. J. Messerly, J. W. Dawson, *Appl. Opt.* 2012, 51, 84.

23- Z. H. Fan, D. J. Harrison, *Anal. Chem.* 1994, 66, 177.

24- A. Berthold, B. Jakoby, M. J. Vellekoop, *Sens. Actuators, A* 1998, 68, 410.

25- *Alloying: Understanding the Basics* (Ed: J. R. Davis), ASM International, Materials Park, OH 2001, 351.

26- F. C. Porter, Zinc Handbook: Properties, Processing and Use *in Design*, CRC Press, Boca Raton, FL 1991.

27- D. R. Lide, CRC Handbook of Chemistry and Physics, 86th edition, Taylor & Francis, London 2005.

28- S. C. Warren-Smith, T. M. Monro, *Opt. Express* 2014, 22, 1480.

29- S.-M. Tseng, C.-L. Chen, *Appl. Opt.* 1992, 31, 3438.

30- Y. Mousli, L. Rouvière, I. Traboulsi, J. Hunel, T. Buffeteau, K. Heuzé, L. Vellutini, E. Genin, *ChemistrySelect* 2018, 3, 7333.

31- N. Al-Hajj, Y. Mousli, A. Miche, V. Humblot, J. Hunel, K. Heuzé, T. Buffeteau, E. Genin, L. Vellutini, *Appl. Surf. Sci.* 2020, 527, 146778.

32- W. Xi, T. F. Scott, C. J. Kloxin, C. N. Bowman, *Adv. Funct. Mater.* 2014, 24, 2572.

33- J. Escorihuela, A. T. M. Marcelis, H. Zuilhof, *Adv. Mater. Interfaces* 2015, 2, 1500135.

34- J. L. Auguste, G. Humbert, S. Leparmentier, M. Kudinova, P. O. Martin, G. Delaizir, K. Schuster, D. Litzkendorf, *Materials* 2014, 7, 6045.

35- Z. Lian, M. Segura, N. Podoliak, N. Feng Xianand White, P. Horak, *Materials* 2014, 7, 5591.

36- C. Strutynski, F. Desevedavy, A. Lemière, J.-C. Jules, G. Gadret, T. Cardinal, F. Smektala, S. Danto, *Opt. Mater. Express* 2017, 7, 1503.

37- C. Hou, X. Jia, L. Wei, S.-C. Tan, X. Zhao, J. D. Joannopoulos, Y. Fink, *Nat. Commun.* 2015, 6, 6248.

38- D. Miklavčič, D. Šemrov, H. Mekid, L. M. Mir, *Biochim. Biophys. Acta, Gen. Subj.* 2000, 1523, 73.

39- D. Miklavcic, S. Corovic, G. Pucihar, N. Pavselj, *EJC Suppl.* 2006, 4, 45.

40- J. C. Travers, W. Chang, J. Nold, N. Y. Joly, P. St. J. Russell, *J. Opt. Soc. Am. B* 2011, 28, A11.

41- K. F. Mak, J. C. Travers, N. Y. Joly, A. Abdolvand, P. S. J. Russell, *Opt. Lett.* 2013, 38, 3592.

42- Y. LeChasseur, S. Dufour, G. Lavertu, C. Bories, M. Deschênes, R. Vallée, Y. De Koninck, *Nat. Methods* 2011, 8, 319.

43- M. Fokine, L. E. Nilsson, Å. Claesson, D. Berlemont, L. Kjellberg, L. Krummenacher, W. Margulis, *Opt. Lett.* 2002, 27, 1643.

44- J. G. Hayashi, R. Lwin, A. Stefani, S. Fleming, B. T. Kuhlmey, A. Argyros, *J. Light Technol.* 2019, 37, 5001.

45- C. Strutynski, L. Teulé-Gay, S. Danto, T. Cardinal, *Sensors* 2020, 20, 2353.

46- N. P. Bansal, R. H. Doremus, Handbook of Glass Properties, Elsevier, NYC, New York 1986.

47- R. W. B. Pearse, A. G. Gaydon, Identification of Molecular Spectra, Chapman And Hall, London 1976.